ChemComm

COMMUNICATION

View Article Online
View Journal

Cite this: DOI: 10.1039/d6cc02515c

Received 23rd April 2026,
Accepted 8th June 2026

DOI: 10.1039/d6cc02515c

rsc.li/chemcomm

Ensemble and single particle analysis of doxorubicin silk nanoparticles

Napaporn Roamcharern,[ab] Panida Punnabhum,[a] Harriet Graham,[a] F. Philipp Seib [acd] and Zahra Rattray *[a]

Adsorption-loaded silk nanoparticles exploit protein electrostatics and β-sheet-rich architecture to achieve high doxorubicin loading and pH-responsive release, while preserving silk structure. Ensemble and single-particle analyses reveal exceptional formulation uniformity, while *in vitro* studies confirm preserved cytotoxicity against MDA-MB-231 human breast cancer cells.

Doxorubicin is a widely used chemotherapeutic agent, yet its clinical utility is limited by cumulative cardiotoxicity and chemoresistance, prompting the development of nanocarriers that have partially mitigated some of these limitations.[1–4] Formulation complexity, heterogenous drug loading, and adverse effects of these formulations, continue to constrain translational performance of doxorubicin nanoparticles.[5] Silk fibroin nanoparticles, distinguished by their β-sheet-rich structure and tuneable surface chemistry, offer favourable physicochemical characteristics,[6–8] including controlled release,[9,10] enhanced internalization and lysosomotropic delivery,[11] and improved solubility.[9,12] Despite growing interest in silk nanoparticles as nanoscale delivery vehicles, the impact of drug loading strategies exploiting these features to govern drug release behaviour remains underexplored.[13–16] Here, we investigate adsorption-based loading of doxorubicin onto pre-formed silk nanoparticles as a chemically defined strategy to spatially confine doxorubicin without disrupting β-sheet-rich protein architecture. We hypothesised that adsorption would preserve silk secondary structure while directly linking protein electrostatics to pH-responsive release behaviour.

Silk nanoparticles prepared by semi-batch antisolvent precipitation formed monodisperse, spherical assemblies with negative surface charge, consistent with β-sheet-rich structure. Adsorption of doxorubicin resulted in high encapsulation efficiency (~90%) without measurable changes in particle size or morphology (Fig. 1a–e, Fig. S2–S4). A modest shift in surface charge toward less negative values was observed, consistent with electrostatic interactions between protonated amines on doxorubicin and anionic silk residues, while retaining colloidal stability. Fourier-transform infrared spectroscopy (FTIR) analysis confirmed retention of β-sheet-dominated secondary structure of

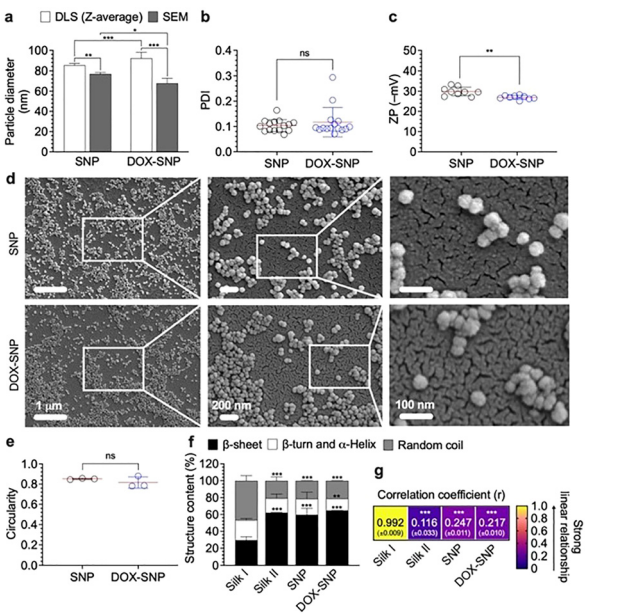

Fig. 1 Physicochemical properties of doxorubicin-loaded silk nanoparticles (DOX-SNPs; 100 μM DOX): (a) Particle diameter; (b) PDI; (c) Zeta potential (ZP); (d) FE-SEM micrographs; (e) Circularity; (f) Secondary structure content; (g) Correlation coefficient (FTIR), determining the linear relationship of IR adsorption spectra using silk I structure as reference. $p < 0.1$(*), $p < 0.01$(**), $p < 0.001$(***), $n = 3$.

[a] *Strathclyde Institute of Pharmacy and Biomedical Sciences, University of Strathclyde, 161 Cathedral St., Glasgow G4 0RE, Scotland, UK. E-mail: zahra.rattray@strath.ac.uk*
[b] *Department of Biotechnology, Faculty of Engineering and Industrial Technology, Silpakorn University, 6, Rajamankha Nai Rd., Amphoe Muang, Nakhon Pathom 73000, Thailand*
[c] *Fraunhofer Institute for Molecular Biology and Applied Ecology, Branch Bioresources, Ohlebergsweg 12, 35392 Giessen, Germany*
[d] *Friedrich Schiller University Jena, Institute of Pharmacy, Department of Pharmaceutics and Biopharmaceutics, Lessingstr. 8, 07743 Jena, Germany*

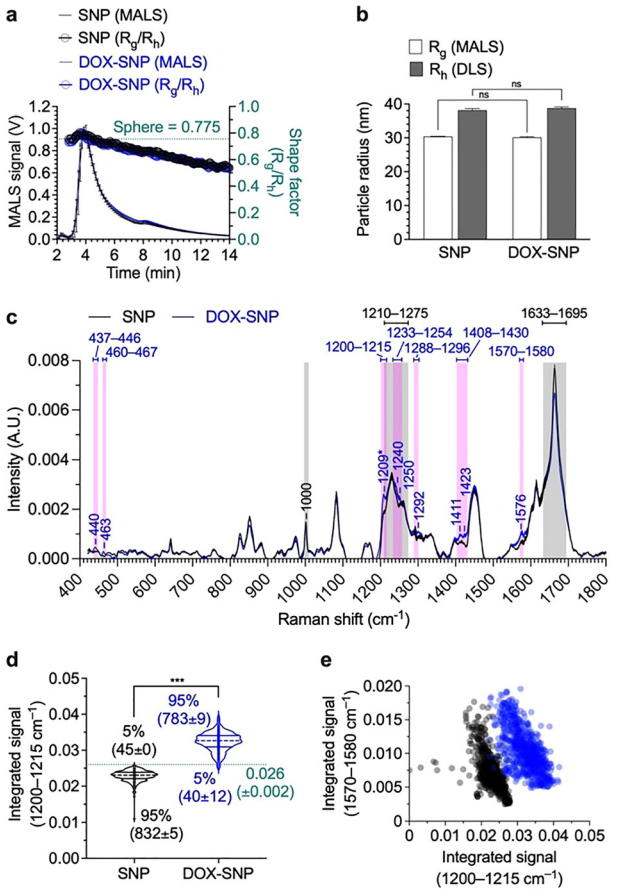

Fig. 2 FI-AF4 fractogram and SPARTA. (a) FI-AF4-MALS aligned with computed shape factor (R_g/R_h). Dotted line indicates ideal spherical shape factor of 0.775. (b) R_g and R_h were obtained from MALS and DLS detector measurements. (c) Overlay of Raman spectra (421–1800 cm^{-1}) for protein (black) and doxorubicin (pink). (d) Integrated Raman signal analysed by the univariate analysis mode. (e) Bivariate analysis, showing a signal intensity correlation of 1200–1215 and 1570–1580 cm^{-1}. $p < 0.1$(*), $p < 0.01$(**), $p < 0.001$(***), $n = 3$.

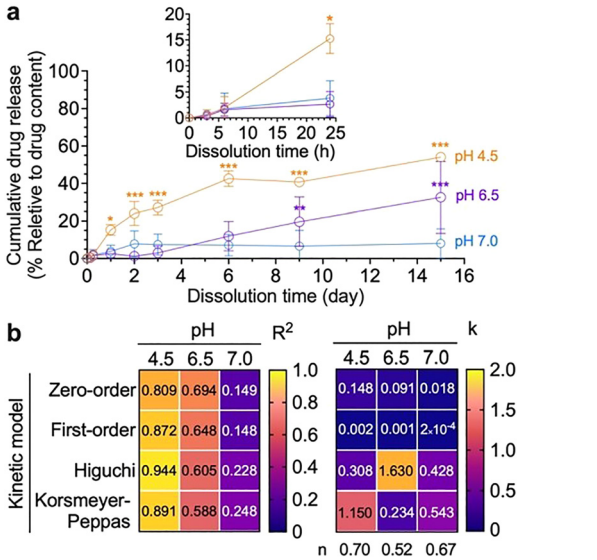

Fig. 3 *In vitro* drug release. Doxorubicin-loaded silk nanoparticles (DOX-SNPs; 100 μM DOX) were prepared at 1.5 mg protein, followed by dialysis against 2 mL of buffer (1× PBS pH 7.0, HEPES buffer pH 6.5, and citrate phosphate buffer pH 4.5) for 15 days; (a) Cumulative drug release; (b) release kinetics. $p < 0.1$(*), $p < 0.01$(**), $p < 0.001$(***), $n = 3$.

the nanoparticles following doxorubicin adsorption. The preservation of silk-like features indicates that doxorubicin remains localised at or near the nanoparticle surface rather than penetrating the β-sheet-rich core (Fig. 1f, g and Fig. S5).[17,18]

This partial constraint is chemically significant, as β-sheet-rich domains regulate particle stability, chain mobility, and diffusion pathways, as β-sheet domains regulate silk chain mobility and diffusion pathways that govern drug retention and release. Formulation integrity and population heterogeneity were assessed using FI-AF4 coupled with MALS, DLS, and spectroscopic detection (Fig. S6). Doxorubicin loading slightly alters nanoparticle size, shape factor, or aggregation behaviour; however, confirming that adsorption effectively preserves nanoparticle morphology (Fig. 2a, b, and Table S1).[19,20]

Single particle automated Raman trapping analysis provided direct evidence of formulation homogeneity. Characteristic doxorubicin Raman signatures were detected in ~95% of individual particles, with strong correlation across multiple diagnostic vibrational bands (Fig. 2c and Table S2, S3). Raman spectra of silk nanoparticles (421 to 1800 cm^{-1}) were dominated by protein features, including amide stretches, and phenylalanine, whereas, doxorubicin features slightly shifted relative to reported values (Fig. 2c and Table S2).[21,22] These changes likely reflect differences in excitation conditions and the local chemical environment.[21] Despite partial overlap between doxorubicin and protein bands, doxorubicin-loaded nanoparticles showed a clear and consistent increase in drug-associated Raman signals across multiple diagnostic peaks (Fig. 2c).

Univariate and bivariate analyses confirmed a distinct separation between empty and drug-loaded particle populations, with particularly strong discrimination at 1209 cm^{-1} (Fig. 2d, e), indicating highly homogeneous drug incorporation (Fig. 2d, e and Fig. S7, S8).[22] A concomitant reduction in Raman intensity at 1660, 850, and 825 cm^{-1} corresponding to the Amide I (C═O) stretch at 1660 cm^{-1} and tyrosine residues at 850 and 825 cm^{-1},[23] suggests localised perturbation of the silk fibroin structure. These changes are consistent with hydrogen bonding between protonated doxorubicin and silk carbonyl groups, together with hydrophobic interactions involving tyrosine residues, supporting the formation of a surface-associated silk-doxorubicin complex (Fig. 2c). This single-particle insight confirms uniform drug distribution, overcoming a key limitation of ensemble-averaged measurements that obscure population heterogeneity. Subtle attenuation of specific protein Raman bands suggests local perturbation of the silk microenvironment upon drug binding, consistent with protein-drug complex formation at the particle surface.[24]

Adsorption-loaded silk nanoparticles exhibited pronounced pH-dependent doxorubicin release under physiologically relevant conditions. Drug release increased systematically with decreasing pH, following the trend pH 7.0 < 6.5 < 4.5, reflecting protonation-driven weakening of electrostatic interactions and increased silk

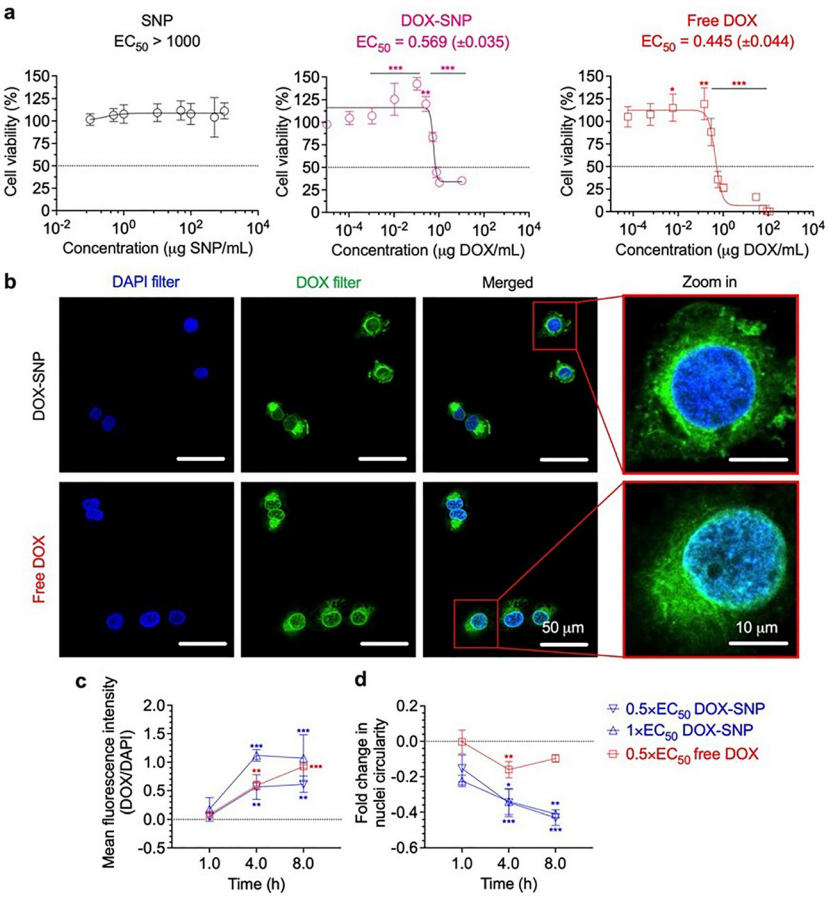

Fig. 4 Cellular responses in MDA-MB-231 cells. Cells were incubated with doxorubicin-loaded silk nanoparticles (DOX-SNPs; 100 μM DOX) for 48 h, followed by the CellTiter-Glo assay; (a) Dose-dependent cytotoxicity of placebo SNPs, DOX-SNPs, and doxorubicin; (b) Confocal images (63×) after 1 h exposure (0.5 × EC_{50}); (c) DOX/DAPI intensity; (d) Fold-change in nuclear circularity after 1–8 h exposure. $p < 0.1$(*), $p < 0.01$(**), $p < 0.001$(***), $n = 3$.

chain mobility below the isoelectric point of silk fibroin (Fig. 3a).[10,25] We speculated that both the physical stability of doxorubicin-loaded silk nanoparticles and dialysis may have influenced the release kinetics, resulting in incomplete doxorubicin release. The physical stability of SNP formulations is pH-dependent.[26] Therefore, doxorubicin encapsulation may further alter formulation stability under dialysis conditions, reducing the release rate and prolonging the release period.

Release kinetics were best described by diffusion-dominated models incorporating polymer relaxation (Higuchi and Korsmeyer-Peppas models), indicating diffusion-controlled release coupled with polymer relaxation (Fig. 3b and Fig. S9).[27,28]

As proof-of-concept evaluation of biological performance, silk nanoparticles were evaluated in MDA-MB-231 triple-negative breast cancer cells. Placebo nanoparticles exhibited negligible cytotoxicity, confirming biocompatibility. In contrast, doxorubicin-loaded nanoparticles demonstrated dose-dependent cytotoxicity comparable to free doxorubicin (Fig. 4a). Confocal imaging revealed time- and concentration-dependent uptake, with intracellular doxorubicin localising in perinuclear regions, consistent with its known mechanism of action. These results confirm that adsorption-mediated loading preserves pharmacological efficacy, while enabling pH-responsive delivery (Fig. 4b–d).

The pH of the cell culture medium was maintained at approximately 7.4 by bicarbonate buffering. Based on the release profile at pH 7.0, only limited doxorubicin release from doxorubicin-loaded silk nanoparticles (~10%) was expected within 48 h of incubation. Together with the proposed cellular uptake mechanism, we hypothesized that doxorubicin-loaded silk nanoparticles were internalized *via* endocytosis and subsequently sequestered to lysosomes. Under these conditions, the acidic lysosomal environment (pH ~ 4.5) may enhance doxorubicin release, potentially increasing cumulative release to ~15% within 48 h (Fig. 3a). Nevertheless, *in vivo* DOX release should be further investigated, as current *in vitro* release methods may not fully reflect the release behaviour of doxorubicin-loaded silk nanoparticles under physiological conditions.

In summary, this study established adsorption as a chemically tractable strategy for loading doxorubicin onto silk nanoparticles, coupling protein electrostatics and β-sheet structure to pH-responsive release while demonstrating high biocompatibility, retention of therapeutic efficacy, and potential selectivity toward cancer cells. Together, these findings support the rational design of tunable silk-based nanocarrier systems for targeted doxorubicin delivery.

Author contributions

NR wrote the manuscript, designed and conducted the experiments, and analysed the data. HG assisted with the use of the confocal microscope. PB assisted with the use of FI-AF4. FPS conceptualized and designed the study and edited the manuscript. ZR conceptualised and designed the study, analysed data, edited the manuscript, and acquired funding.

Conflicts of interest

There are no conflicts to declare.

Abbreviations

B. mori	Bombyx mori
DAPI	4′,6-diamidino-2-phenylindole
DLS	Dynamic light scattering
DOX	Doxorubicin
DOX-SNP	Doxorubicin-loaded silk nanoparticle
EC_{50}	Half-maximal effective concentration
ELS	Electrophoretic light scattering
FE-SEM	Field-emission scanning electron microscopy
FI-AF4	Frit-inlet asymmetric flow field-flow fractionation
FTIR	Fourier-transform infrared
IPA	Isopropanol
LiBr	Lithium bromide
MALS	Multiangle light scattering
Na_2CO_3	Sodium carbonate
PDI	Polydispersity index
R_g	Radius of gyration
R_h	Hydrodynamic radius
SNP	Silk nanoparticle
SPARTA	Single particle automated trapping analysis
UV	Ultra-violet
X-Flow	Cross-flow
ZP	Zeta potential

Data availability

All data associated with this work are included in the supplementary information or can be accessed at https://doi.org/10.15129/ed1bb0a8-6eff-434f-8355-ac5ede92b5b9.

Supplementary information (SI) is available. See DOI: https://doi.org/10.1039/d6cc02515c.

Acknowledgements

We thank Catherine Saunders for providing access to the SPARTA system. NR acknowledges funding from the Office of Educational Affairs, UK; the Royal Thai Embassy, Thailand; and the Office of the Civil Service Commission, Thailand, which provided a PhD scholarship. The authors acknowledge that the scanning electron microscopy work was carried out at the Advanced Materials Research Laboratory at the University of Strathclyde. ZR and FPS thank the Engineering and Physical Sciences Research Council (EP/V028960/1) for financial support.

References

1 A. Bisht, D. Avinash, K. K. Sahu, P. Patel, G. Das Gupta and B. D. Kurmi, *Drug Delivery Transl. Res.*, 2025, **15**, 102–133.
2 S. A. L. Matthew and F. P. Seib, *Adv. Ther.*, 2025, **8**, 2400130.
3 I. C. Jones and C. R. Dass, *J. Pharm. Pharmacol.*, 2022, **74**, 1677–1688.
4 U. Bulbake, S. Doppalapudi, N. Kommineni and W. Khan, *Pharmaceutics*, 2017, **9**, 12.
5 A. Fukuda, K. Tahara, Y. Hane, T. Matsui, S. Sasaoka, H. Hatahira, Y. Motooka, S. Hasegawa, M. Naganuma and J. Abe, *PLoS One*, 2017, **12**, e0185654.
6 M. A. Asensio Ruiz, Á. Alonso García, M. D. L. L. Bravo-Ferrer Moreno, I. Cebreiros-López, J. A. Noguera-Velasco, A. A. Lozano-Pérez and T. Martínez Martínez, *Pharmaceuticals*, 2023, **16**, 248.
7 S. Gou, Y. Huang, Y. Wan, Y. Ma, X. Zhou, X. Tong, J. Huang, Y. Kang, G. Pan and F. Dai, *Biomaterials*, 2019, **212**, 39–54.
8 F. P. Seib, *AIMS Bioeng.*, 2017, **4**, 239–258.
9 J. Kundu, Y.-I. Chung, Y. H. Kim, G. Tae and S. C. Kundu, *Int. J. Pharm.*, 2010, **388**, 242–250.
10 F. P. Seib, G. T. Jones, J. Rnjak-Kovacina, Y. Lin and D. L. Kaplan, *Adv. Healthcare Mater.*, 2013, **2**, 1606–1611.
11 J. D. Totten, T. Wongpinyochit and F. P. Seib, *J. Drug Targeting*, 2017, **25**, 865–872.
12 S. Shaidani, C. Jacobus, J. K. Sahoo, K. Harrington, H. Johnson, O. Foster, S. Cui, O. Hasturk, T. Falcucci and Y. Chen, *ACS Appl. Nano Mater.*, 2023, **6**, 18967–18977.
13 B. Yu, Y. Li, Y. Lin, Y. Zhu, T. Hao, Y. Wu, Z. Sun, X. Yang and H. Xu, *Front. Pharmacol.*, 2023, **13**, 1071868.
14 S. Bhattacharjee and D. J. Brayden, *Expert Opin. Drug Discovery*, 2021, **16**, 235–254.
15 A. Bhadran, H. Polara, G. K. Babanyinah, S. Baburaj and M. C. Stefan, *Cancers*, 2025, **17**, 2303.
16 T. N. Saeed, A. F. Al-Hussainy, G. Sanghvi, S. Ballal, A. Singh, T. Sudhakar, S. Mishra, A. Kubaev, S. G. Taher and M. Alwan, *J. Drug Delivery Sci. Technol.*, 2025, 107649.
17 W. Cai, M. Guo, X. Weng, W. Zhang and Z. Chen, *Mater. Sci. Eng., C*, 2019, **98**, 65–73.
18 C. Racles, M.-F. Zaltariov, D. Peptanariu, T. Vasiliu and M. Cazacu, *Nanomaterials*, 2022, **12**, 1823.
19 M. Wang, W. Zhang, L. Yang, Y. Li, H. Zheng and H. Dou, *Food Chem.:X*, 2024, **22**, 101267.
20 A. M. Striegel, *Macromolecular separation science*, Springer Nature, 2025.
21 P. V. A. Pessanha and A. C. Sant'Ana, *J. Braz. Chem. Soc.*, 2025, **36**, e20250121.
22 R. Zhang, J. Zhu, D. Sun, J. Li, L. Yao, S. Meng, Y. Li, Y. Dang and K. Wang, *Micromachines*, 2022, **13**, 940.
23 J. Guo, W. Cai, B. Du, M. Qian and Z. Sun, *Biophys. Chem.*, 2009, **140**, 57–61.
24 J. Penders, I. J. Pence, C. C. Horgan, M. S. Bergholt, C. S. Wood, A. Najer, U. Kauscher, A. Nagelkerke and M. M. Stevens, *Nat. Commun.*, 2018, **9**, 4256.
25 C. W. P. Foo, E. Bini, J. Hensman, D. P. Knight, R. V. Lewis and D. L. Kaplan, *Appl. Phys. A*, 2006, **82**, 223–233.
26 N. Roamcharern, P. Punnabhum, F. P. Seib and Z. Rattray, *Nanoscale Adv.*, 2025, **7**, 5519–5535.
27 A. Szepes, Z. Makai, C. Blümer, K. Mäder, P. Kása Jr and P. Szabó-Révész, *Carbohydr. Polym.*, 2008, **72**, 571–578.
28 P. I. P. Soares, A. I. Sousa, J. C. Silva, I. M. M. Ferreira, C. M. M. Novo and J. P. Borges, *Carbohydr. Polym.*, 2016, **147**, 304–312.

